Subconductor Partition Algorithm for the Fast Computation of Cable Impedance

Isaí Diaz, Felipe Uribe, Pavel Zuniga, Marcos Padilla, Juan Ramón Morales, Fernando Elizalde

***Abstract*—This work proposes a fast, accurate, and numerically efficient algorithm using the partial subconductor division method to estimate the frequency-dependent parameters of electrical power cables with non-axial cross-section. The computer execution time is drastically reduced while maintaining a high numerical accuracy by scaling the subconductor dimensions and compensating the error introduced by the shape of the subconductor.**

Finally, the results are validated through Schelkunoff's coaxial transmission line theory for a concentric cable and with the finite element method interfacing boundary layer properties between insulator/conductor for a segmental three-phase cable.

***Keywords*: Numerical methods and modeling, Transmission line analysis, Cables, Finite element method, frequency dependent.**

I. Introduction

New power cable technologies require continuous innovation in design techniques to face the modern industry challenges in renewable energy projects. To support the growing electrical power demand, each day more wind farms are installed offshore and transmit electrical energy to the mainland using submarine power cables to connect high-voltage direct current (HVDC) converters [1-5]. Some of the new technologies in power cables are based on segmental, sectorial or umbilical geometries, and the pipe trench where these are installed combines power cables, optical fiber for communications, ground conductors, and linking pilot cables of highway bridges. Unfortunately, no well-accepted routine or methodology is available in EMTP-type software to estimate electrical parameters in per unit length (pul) of the series-impedance (Z) for these new power cable geometries [6-15]. In most EMTP-type software, the studies are typically restricted to concentric cables that often already have predefined configurations and specific datasets for conductor parameter settings [16].

Given these constraints, one alternative is to partition the original image of the cable into several subconductors with a much smaller cross-section, utilizing simple geometrical shapes such as squares, circles, or rectangles. When combined with modern computer resources, this approach can offer promising possibilities [17-28]. This approach also allows to select certain parameters of the algorithm, such as the discretization resolution, the shape of the subconductor, or include the skin and proximity effects in the model.

On the other hand, there is specialized software designed primarily for solving electromagnetic field problems. One such method is the finite element method (FEM), which operates like a black box and often requires guidance from experienced users [29-35]. Therefore, having alternative methods to estimate electrical parameters of non-axial cables can be a promising option for EMTP-type software.

However, the spatial discretization of a cross-section cable, *e.g.* the resolution as a function of the skin-effect depth, and the necessary refinements of a subconductors partition (a type of optimization process) results in a substantial increase in computational burden, which in consequence can make the process very long and time-consuming [17-27]. It is probably because of this drawback, that the subconductor partition algorithms are seldom studied or used to estimate electrical parameters of power cables with non-axial cross-section for electromagnetic transient or harmonic analysis.

This paper presents a fast and accurate subconductor partition algorithm to estimate the frequency dependent impedance of electrical cables. The MATLAB [36] implemented algorithm scales the subconductor dimensions and compensates the error introduced by the shape of the subconductor to reduce the computer execution time as the number of subconductors increases [22-26].

II. Subconductor Partition Formulation

In subconductor partition algorithms, the voltages V_n and currents I_n are related through the well-known First Telegrapher Equation, which describes the voltage and current relation of a transmission system through the following square matrix system

$$-\frac{d}{dx}\begin{bmatrix}V_1\\V_2\\\vdots\\V_n\end{bmatrix}=\begin{bmatrix}R_{11}&0&\dots&0\\0&R_{22}&\cdots&\vdots\\\vdots&\vdots&\ddots&\vdots\\0&\cdots&\cdots&R_{nn}\end{bmatrix}\begin{bmatrix}I_1\\I_2\\\vdots\\I_n\end{bmatrix}+\cdots$$

$$\cdots+j\omega\begin{bmatrix}L_{11}&L_{12}&\dots&L_{1n}\\L_{21}&L_{22}&\dots&L_{2n}\\\vdots&\vdots&\ddots&\vdots\\L_{n1}&L_{n2}&\dots&L_{nn}\end{bmatrix}\cdot\begin{bmatrix}I_1\\I_2\\\vdots\\I_n\end{bmatrix} \quad (1)$$

$$for\ n=1,2,3,\dots,N_{subc}$$

This work was supported in part by The University of Guadalajara.

I. Diaz, F. A. Uribe, P. Zuniga, and J. R. Morales are with The University of Guadalajara, CUCEI, Guadalajara, Jalisco, Mexico PC. 44430 (felipe.uribe@academicos.udg.mx).

M. Padilla is with CENACE, Occidental Region, Jal. México.

Paper submitted to the International Conference on Power Systems Transients (IPST2025) in Guadalajara, Mexico, June 8-12, 2025.

where N_{subc} is the number of subconductors [8, 17]; R_{nn} and L_{nn} in the main diagonal are the self-resistive and self-inductive components related to the skin effect; L_{nm} is the magnetic flux coupling between conductors; and all parameters in (1) are defined in per unit length (pul) [9-15].

III. Scaling the Subconductor Dimensions

The subconductor dimensions are scaled on the assumption that processing a spatially reduced cable with fewer subconductors is more computationally efficient than handling the cable in its original size. This method reduces the computational demands and processing time by proportionally decreasing the dimensions of the cross-section of a cable while maintaining high accuracy.

As a graphical example, the left-hand side of Fig. 1 shows an electrical cable in its original size, and the right-hand side of Fig. 1 shows the scaled 2:1 version; both are partitioned in square-shape subconductors. When choosing a resolution of 8 sub/in, the conductor subdivision method requires 10s of computer execution time, whereas when using the scaled version, it only requires 1s. The root mean square error (RMSE) when using the conductor subdivision method with the cable in its original size is 0.015Ω for R and approximately 0.008H for L, whereas when using the scaled version, the values are 0.013Ω for R and approximately 0.005H for L. On the other hand, the correlation index for the conductor subdivision method with the cable in its original size is 0.3 for R and approximately 0.6 for L, whereas for the scaled version is nearly 0.5 for R and 0.75 for L. For the RMSE and correlation index, the reference data is taken from an analytical simulation using Schelkunoff's theory [16].

A. Geometric scaling of the cross-section of a cable

In subconductor partition algorithms it is considered that the current density is uniformly distributed in each of the subconductors [17-20]. The numerical computation of R and L for the i^{th} subconductor, applying the corresponding scaling factor, is related to the analytical formulas described in [16] with the following parameters

$$R_i = \frac{\rho_i}{A_i} \propto \frac{\rho_i}{A'_i}, \tag{2}$$

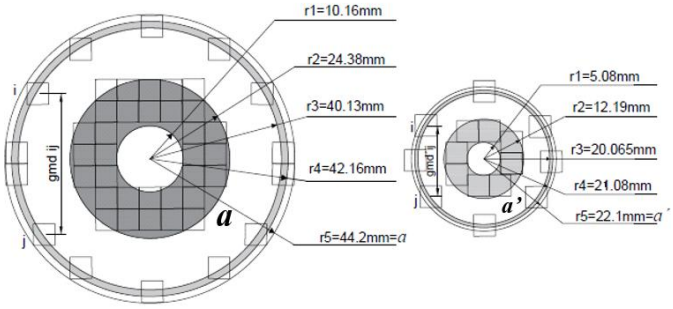

Fig. 1 Coaxial electrical cable with the a 2:1 scaled version

where ρ_i is the conductor material resistivity, A_i is the area of the i^{th} subconductor, and the proportional variation of the resistance is based on the following scaled relation

$$A'_i = A_i S_f, \tag{3}$$

where S_f is the scaling factor.

In addition, the following relation between the cable radius a, that in this case is also the fictitious ground-return, and the geometric mean distance gmd_i of the i^{th} subconductor is satisfied proportionally according to [8, 17]

$$\frac{a}{gmd_i} = \frac{a'}{gmd'_i}, \tag{4}$$

where the terms in the right hand-side are related to the scaled cable. Preserving equal proportions for the inductances, we have [17-23]

$$L_{ii} = \frac{\mu_0}{2\pi} ln\left(\frac{a}{gmd_i}\right) = \frac{\mu_0}{2\pi} ln\left(\frac{a'}{gmd'_i}\right), \tag{5}$$

$$L_{ij} = \frac{\mu_0}{2\pi} ln\left(\frac{a}{gmd_{ij}}\right) = \frac{\mu_0}{2\pi} ln\left(\frac{a'}{gmd'_{ij}}\right), \tag{6}$$

where L_{ii} is the self-inductance (H/m) of the i^{th} subconductor, L_{ij} is the mutual inductance (H/m) between the i^{th} and the j^{th} subconductors, and ⌈0 is the vacuum permeability. For the real-size conductor in the left-hand side of Fig. 1, gmd_i is the geometric-mean distance of the i^{th} subconductor and gmd_{ij} is the geometric-mean distance between the i^{th} and the j^{th} subconductors. For the scaled-size conductor in the right-hand side of Fig. 1, gmd_i' is the geometric-mean distance of the i^{th} scaled subconductor and gmd_{ij}' is the geometric-mean distance between the i^{th} and the j^{th} scaled subconductors.

Among the main features of the computer performance of an algorithm is the complexity, accuracy, and execution time [36].

In typical analyses of electromagnetic transients or harmonic induction studies, the matrix system in (1), with frequency-dependent electrical parameters represented by $Z(\omega)=R(\omega)+j\omega L(\omega)$, has to be solved at least 1,000 times for a voltage response observation time of 1ms, sampled at 1μs; this is related to the expression [36-38]

$$N = \frac{T_{obs}}{\Delta t}, \tag{7}$$

where N is the number of samples, T_{obs} is the time observation window and Δt is the sampling time-step.

Table 1 shows the estimated values of R and L with the Schelkunoff's theory [16], the conductor subdivision algorithm in [8, 17], and the proposed scaled subconductor partition algorithm using 5 frequency samples between 10Hz<f<100kHz and a 16 sub/in resolution implemented in MATLAB [36].

Fig. 2 shows a qualitative and quantitative accuracy analysis of the proposed technique as a function of the subconductor resolution; note that Table I shows a particular case of Fig. 2 when the resolution is 16 sub/in.

TABLE I

RESISTANCES AND INDUCTANCES OF THE CURRENT LOOP BETWEEN CORE AND SHEATH OF THE CONCENTRIC CABLE FOR A RESOLUTION OF 16 SUB/IN

Parameter	*f* (Hz)	Schelkunoff	Conductor Subdivision	Proposed algorithm
R(mΩ/km)	10	416.1	421.4	420.1
	100	422.2	426.8	425.4
	1k	471.6	469.7	470.5
	10k	644.8	645.4	643.2
	100k	1835.0	1826.0	1833.6
L(mH/km)	10	0.1397	0.1392	0.1393
	100	0.1350	0.1359	0.1335
	1k	0.1142	0.1154	0.1150
	10k	0.1065	0.1073	0.1069
	100k	0.1026	0.1043	0.1035

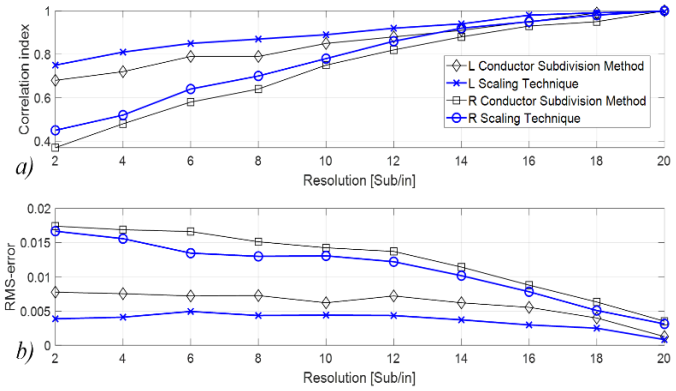

Fig. 2 Qualitative and quantitative accuracy analysis of the conductor subdivision algorithm in [8, 17] and the proposed scaled subconductor partition algorithm as a function of the resolution: a) correlation index and b) RMSE [34].

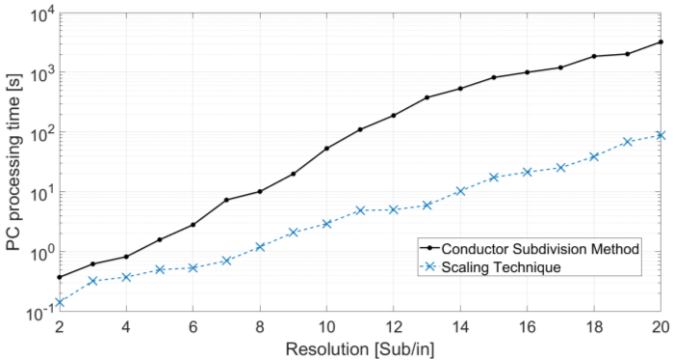

Fig. 3 Computer execution time as a function of the subconductor resolution.

The results in Fig. 2a are quantitative because the correlation factor is an index that represents how much the data vector of the proposed scaled subconductor partition algorithm is similar to the data vector of the conductor subdivision algorithm in [8, 17]. In the optimal case the two vectors are orthogonal and their inner or dot product equals 0, which means they are identical and their correlation index is 1.

The results in Fig. 2b are qualitative because the RMSE yields a number relative to the accuracy of the proposed scaled subconductor partition algorithm to the conductor subdivision algorithm in [8, 17]. As can be seen, the proposed algorithm has an RMSE slightly lower than that of the conductor subdivision method for all the resolution range.

On the other hand, the results in Fig. 3 compare the computer execution time for different resolution values of the proposed scaled subconductor partition algorithm and the conductor subdivision algorithm. As can be noticed, the computer execution time is always lower for the proposed algorithm, and the difference at high resolutions is higher than one order of magnitude. The results in Fig. 3 were obtained using a Windows 64-bit PC with an Intel® Core™ i-7 3770 CPU @ 3.40GHz and 16 GB of RAM.

B. Compensation of the Error Because of the Shape of a Subconductor

Additionally, to scaling the subconductor partition, the shape of the subconductor presents an error that has to be compensated. Consider Fig. 4a that presents the superposition of circular subconductors over square ones with a resolution of 4 Sub/in across the transversal section of a cable; the error area between the two shapes is plotted in Fig. 4b as a function of the resolution. The figure shows that the error decreases as the resolution increases, indicating that, at high resolutions, it is less critical whether to use subconductors with square or circular shape.

a. Square Shape

To estimate the resistance and inductance of a square shape subconductor, the approximate formulation is [16-26, 30]

$$R_{dc_i} = \frac{\rho_i}{A_i} \tag{8}$$

$$L_{ii} = \frac{\mu_0}{2\pi} ln\left(\frac{a}{D_i}\right) \tag{9}$$

$$L_{ij} = \frac{\mu_0}{2\pi} ln\left(\frac{a}{D_{ij}}\right), \tag{10}$$

where a is the fictitious common return that encloses the external radius of the conductor, $D_i = 0.44705l$, and

$$D_{ij} = ln\left(gmd_{ij}\right) = \frac{1}{A_i A_j}\int_{A_i}\int_{A_j} ln\left(\tau\right) dA_i dA_j \tag{11}$$

where A_i is the area of each subconductor in square inches, and l is the length of a square subconductor, as shown in Fig. 4b.

Since D_{ij} is hard to compute, the following expression is used

$$D_{ij} = \sqrt{(x_2^2 - x_1^2) + (y_2^2 - y_1^2)} * 1.065 \tag{12}$$

b. Circular Shape

The self and mutual inductances and the *gmd* for circular sub conductors are equivalent to [21-28]

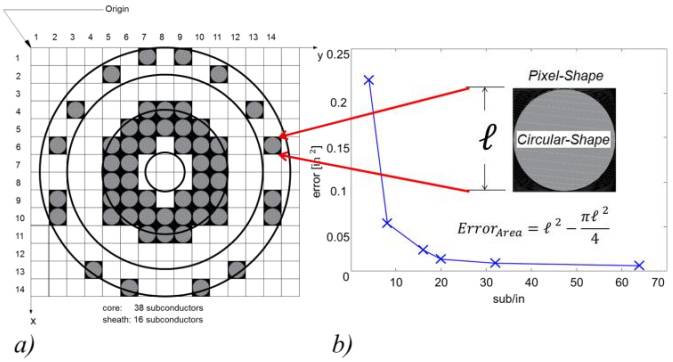

Fig. 4. Discretization superposition using circular and square shapes with 4 Sub/in. a) Discretized image. b) Error of both shapes at six different resolutions.

$$L_{ii} = \frac{\mu_o}{2\pi} ln\left(\frac{D^2{}_{iq}}{D_i D_q}\right) \tag{13}$$

$$L_{ij} = \frac{\mu_o}{2\pi} ln\left(\frac{D_{iq} D_{jq}}{D_q D_{ij}}\right) \tag{14}$$

where D_{iq} is the mutual *gmd* between two circles, and for one circle is $D_i = r_i e^{-\mu_i/4}$ with $\mu_i = 1$.

To use circular sub conductors instead of square ones in the image of Fig. 4a, two types of errors have to be compensated. The first one is due to the differences in the area between a circular and a square subdivision as a function of the resolution (plot in Fig. 4b). This is corrected using the error formula shown in Fig. 4b, which represents the error between a square and a circle. The second one is due to the use of the approximate formula (12) for calculating the *gmd* of square-shaped subconductors [21-28, 31, 33].

This error is corrected using D_{iq} and D_i instead of (12) when circular-shaped subconductors are employed. According to [22-25], all subconductors inherently introduce this type of error except for the case of two adjacent circular subconductors.

The impact of compensating this error is shown in Fig. 5 for a spatial resolution of 20 sub/in for the *R* and *L* loop impedances formed between the sheath and core of the cable in Fig. 4a; the results are obtained from the analytical solution using Schelkunoff's theory, the proposed algorithm with square subconductors, and the proposed algorithm with circle subconductors compensating the shape error.

From Fig. 5a, the correction of *R* indicates that the resistance increases as the area of the subconductor decreases, in agreement with (8) [22-25]. This verifies that the calculation of *R* using circular subconductors with error correction is closer to the analytical solution than the one achieved using square subconductors.

Fig. 5b shows a similar behavior when using circular subconductors and compensating the error to calculate *L*, comparing the results against the analytical Schelkunoff's solution [22-26]. The results indicate that the magnetic flux inside the circular subconductors is slightly higher in magnitude than the one in the square-shaped ones. This occurs when the geometric size of the subconductor is lower than or equal to the width of $\delta \approx \sqrt{\rho/f}$ at a given frequency [22].

IV. Parameter Estimation for Segmental Cables

For concentric power cables, the electrical parameters are calculated according to Schelkunoff's theory for a determined number of time-frequency samples in the Laplace domain [21-24, 25, 37, 38]. However, Schelkunoff's theory cannot be used when the physical geometry of a three-phase electrical power cable is segmental, as the one shown in Fig. 6 with the material properties given in Table II.

Thus, the electrical parameters have to be estimated using other means when searching for validation, for example, numerical methods. Since no analytical solution is available for segmental cables, the FEM is implemented in the professional software COMSOL [29] to validate the proposed scaled algorithm with shape error correction. In addition, and for illustrative purposes, Fig. 7 shows a 3D view of the bitmap image implemented in MATLAB [36] of the segmental electrical cross-section power cable in Fig. 6 [22].

As can be observed in this figure, the pixel information of each of the segmental nuclei and the external sheath subconductor components can be easily identified, giving an idea of the number of subconductors used to process the given data at a specific resolution; for this numerical representation we use a resolution of 46 sub/in.

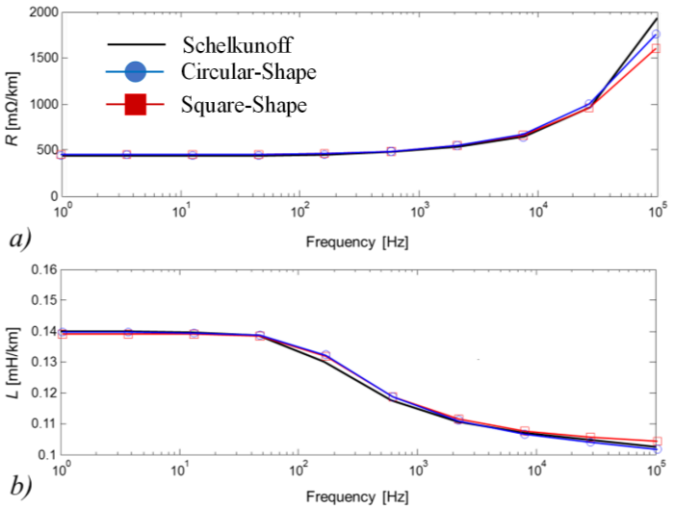

Fig. 5. Loop impedance between the core and sheath of cable in Fig. 5a using a resolution of 20 sub/in. a) resistance and b) inductance.

TABLE II
Conductor Parameters for Power Segmental Cable

Conductors	σ (s/mm)	μ_r
Core (each)	58000	–
External sheath	1100	–
Insulator	0	1

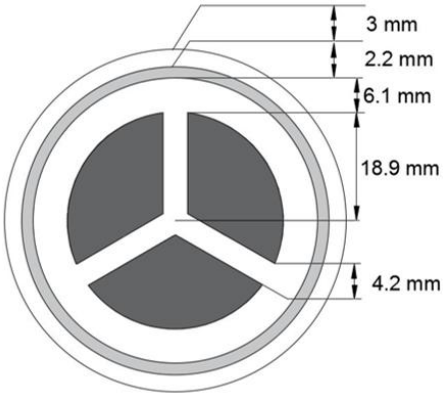

Fig. 6. Three-phase segmental cable cross-section.

The edges of the three core conductors in fig. 7 are represented in red, orange, and green colors, while the dielectric materials of the internal and external insulators of the cable are represented in blue color.

When using an FEM, meshing is one of the fundamental steps in the simulation process, as the results are highly dependent on the appropriate number of elements used. Selecting an excessively refined mesh can lead to a significant increase in computational resource usage, making the mesh inefficient and resulting in longer computer execution times; conversely, a low-resolution mesh can produce inaccurate results.

In areas where electromagnetic quantities vary significantly, such as currents and flux densities, refining the mesh is essential. The number of elements in the mesh is determined based on the skin depth and the frequency range of the parameters. The mesh depicted in Fig. 8 was created using the boundary layer meshing technique comprising 13,368 elements at a test frequency f of 60 kHz, and is applied to each core conductor considering the resistivity of the material and the depth of the skin effect δ(m) calculated using [13-15, 28]

$$\delta \approx 503 \cdot \sqrt{\frac{\rho}{f}} \tag{15}$$

The intensity of the magnetic flux in each core conductor of the cable is obtained exciting the three cores at the same time with a potential of 1V. In this case, the return current is negative and its magnitude is equivalent to the sum of the three core conductor currents. The distribution of the magnetic flux density at a frequency of 60kHz is shown in Fig. 9, where it is evident that, because of the shape of the core conductors, the magnetic flux density is confined into the outer sheath of each core conductor of the cable; this is a particular behavior of the combination of skin and proximity effects in the conductors.

Fig. 10 shows the loop resistances and inductances for the self and mutual components between the cores and the sheath of the segmental cable applying the proposed scaled algorithm with circular and square subconductors, against the FEM [22, 29]; the shape error compensation formulas are used when partitioning in circular subconductors.

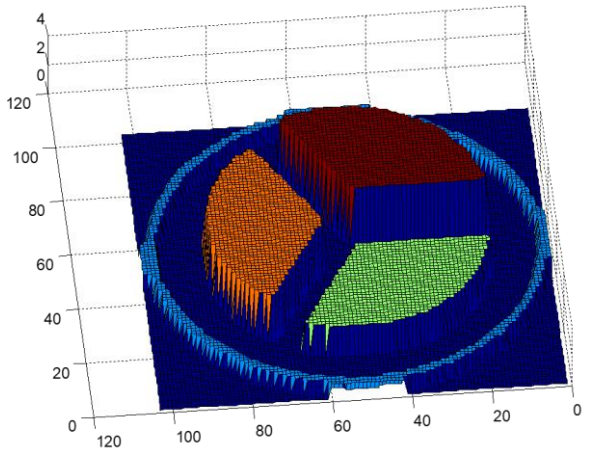

Fig. 7. Illustrative 3D view of the bitmap image of the segmental cable.

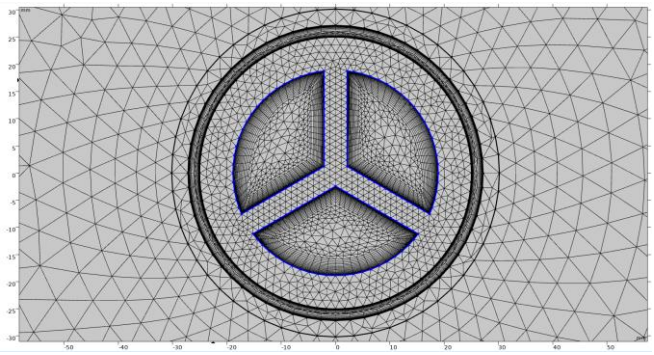

Fig. 8 Mesh generated with FEM using COMSOL using boundary layer meshing with 13368 elements for the segmental cable in Fig. 8.

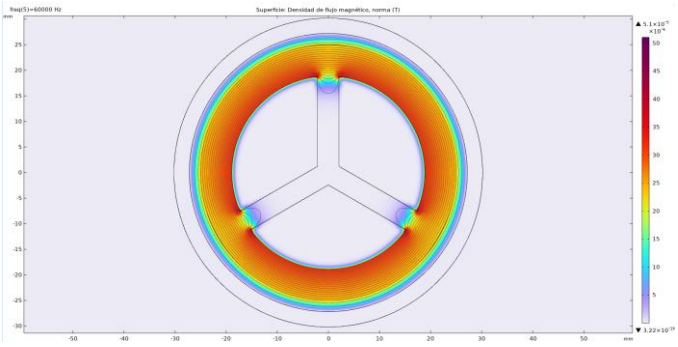

Fig. 9 Magnetic flux density distribution at 60kHz obtained with FEM [34].

As can be seen in Fig. 10a, the magnitude of the loop-resistance increases with the frequency because the effective area of the current density is reduced accordingly to the skin and proximity effects. On the other hand, in Fig. 10b the magnitude of the loop-inductance decreases with the frequency because the magnetic flux is reduced as the effective area of the current density in the conductor decreases [24-27]. It can be seen from Fig. 10 that the conductor subdivision method, for circular and square shapes, and the FEM-based results are in good agreement for the self and mutual resistances and inductances. The relative error for the self and mutual loop-impedance for six samples, each one a decade apart and inside the frequency range 1Hz<f<100kHz, are given in Tables III and IV. The relative error between curves is calculated with

$$\varepsilon_{rel}^{\%} = \left|1 - \frac{f_{approx}}{f_{exact}}\right| \times 100 \quad (16)$$

where f_{approx} is the solution using the FEM and f_{exact} is the proposed scaled algorithm with circular subconductors and shape error correction. It is easy to see from Tables III and IV that the relative error between the proposed scaled algorithm and the FEM is low, which confirms the effectiveness of the proposal.

V. Transient Voltage Response of an Electrical Three-phase Segmental Cable

The electromagnetic transient voltage response at the remote-end of the electrical segmental cable in Fig. 6 is synthesized using the estimated parameters with the proposed scaled algorithm and the FEM through the Numerical Laplace Transform (NLT) implemented in MATLAB [36, 37, 38]. In this study case the cable has a length of 10mi (≈16km) and is buried at a depth of 0.76m in a soil with a resistivity of ρ=100Ωm. Only core 1 is energized with a unit step of voltage at the sending end, thus the transient voltage response at the receiving end of core 1 and the induced cores 2, 3 and sheath are measured.

Fig. 11a shows the transient voltage at the receiving end of core 1, and Fig. 11b shows the induced voltage responses at the core 3 and the sheath. As expected, the overshoot is maximum at the receiving end of core 1, achieving a magnitude of 1.734 pu; whereas a maximum overvoltage magnitude of 0.5402 pu is observed at the initial wave-front of core 1. The propagated voltage is estimated considering the frequency-dependent parameters of the cable.

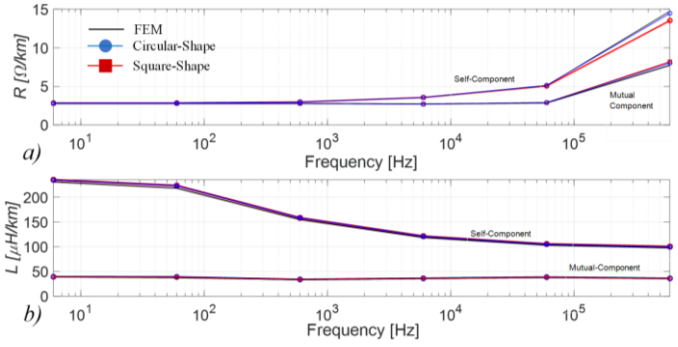

Fig. 10 Loop impedance between the core and sheath of the cable in Fig. 7 using the proposed scaled algorithm with square and circular subconductors, and compared against the FEM. a) resistance and b) inductance.

TABLE III
Self-Loop Impedance Cable Fig. 7 Resolution of 46 Sub/in.

Parameter	*f* (Hz)	FEM	Proposed algorithm	Relative Error(%)
R (Ω/m)	6	0.00284	0.002839	0.039719
	60	0.00285	0.002849	0.030065
	600	0.002967	0.002968	0.042023
	6k	0.003535	0.003557	0.632206
	60k	0.005088	0.005053	0.690415
	600k	0.014731	0.014332	2.708455
	640k	0.015226	0.014781	2.924796
L (H/m)	6	2.31E-07	2.35E-07	1.910963
	60	2.18E-07	2.24E-07	2.400467
	600	1.55E-07	1.58E-07	2.354003
	6k	1.18E-07	1.21E-07	2.357915
	60k	1.03E-07	1.05E-07	2.376004
	600k	9.76E-08	1.00E-07	2.698865
	640k	9.75E-08	1.00E-07	2.709231

TABLE IV
Mutual-Loop Impedance Cable Fig. 7 Resolution of 46 Sub/in.

Parameter	*f* (Hz)	FEM	Proposed algorithm	Relative Error (%)
R(Ω/m)	6	0.002782	0.002781	0.039297
	60	0.002783	0.002782	0.03573
	600	0.002783	0.002783	0.001852
	6k	0.002705	0.002699	0.221935
	60k	0.002846	0.002875	1.015144
	600k	0.007723	0.007758	0.446325
	640k	0.007983	0.007956	0.329252
L(H/m)	6	3.93E-08	3.94E-08	0.20384
	60	3.77E-08	3.90E-08	3.561305
	600	3.36E-08	3.39E-08	0.818055
	6k	3.59E-08	3.61E-08	0.659637
	60k	3.80E-08	3.85E-08	1.362527
	600k	3.59E-08	3.60E-08	0.234113
	640k	3.59E-08	3.60E-08	0.222434

VI. Conclusions

This paper presents a scaled subconductor partition algorithm with shape error correction to enhance computational performance of conductor subdivision numerical methods for estimating electrical parameters of three-phase power cables. The computer execution time with the proposed algorithm is drastically reduced, especially when the resolution of the subconductors increases, and for the values shown in this work can be higher than one order of magnitude compared to other techniques. This accelerates computer calculations, and consequently reduces the numerical complexity of the algorithm. The correction of the error due to the shape of the subconductor directly impacts the estimated values of *R* and *L* for the power cable as a function of the resolution. Although the error is mainly due to the area reduction of the *gmd* calculation, which is higher for square geometries when compared to circular ones.

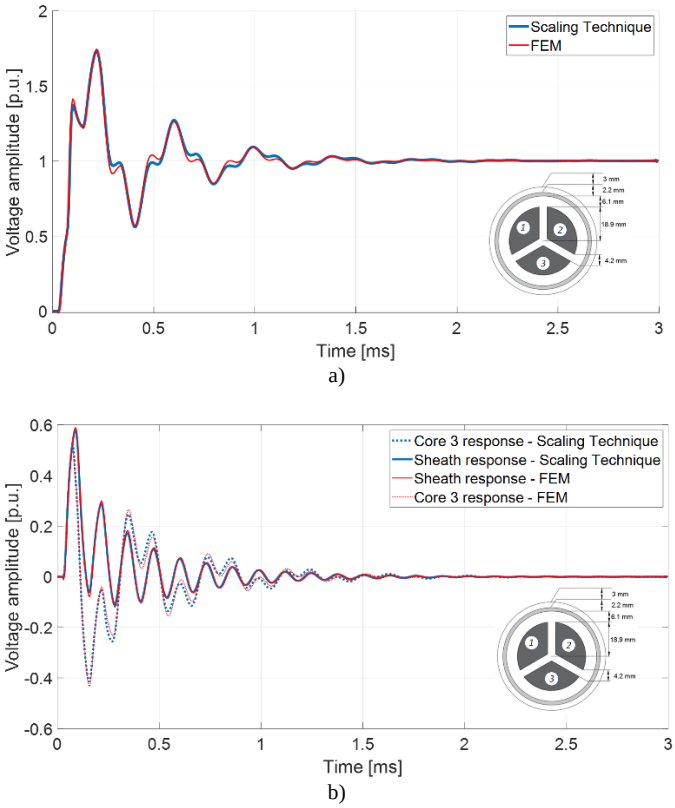

Fig. 11. Transient overvoltages synthesized with NLT using the proposed algorithm and the FEM. a) voltage response at the receiving end. b) induced voltages of core 3 and the sheath.

VII. References

[1] T. Wood, D. E. Macpherson, C. Smith, and S. Finney, "HVDC networks for offshore wind power: Current ripple and cables", 10th IET International Conference on AC and DC Power Transmission (ACDC 2012), Birmingham, 2012, pp. 1-6. doi: 10.1049/cp.2012.2002.

[2] A. J. Urquhart and M. Thomson, "Series impedance of distribution cables with sector-shaped conductors," in IET Generation, Transmission & Distribution, vol. 9, no. 16, pp. 2679-2685, 12 3 2015. doi: 10.1049/iet-gtd.2015.0546.

[3] S. J. Sutton, "High-stress wet aging of cable dielectrics-meeting new challenges", in IEEE Electrical Insulation Magazine, vol. 33, no. 1, pp. 7-14, January-February 2017. doi: 10.1109/MEI.2017.7804311.

[4] A. Apostolov and J. Raymond, "The Electric Power Systems of the Future: Still Progress to be Made [In my View]," IEEE Power and Energy Magazine, vol. 22, no. 3, pp. 112–116, 2024, doi: 10.1109/mpe.2024.3366503.

[5] T. Otani, "Power grids achieving carbon neutrality with a reduced labor force: Energy management and automation systems cooperation," IEEE Power and Energy Magazine, vol. 22, no. 3, pp. 20–28, 2024, doi: 10.1109/mpe.2023.3344557.

[6] A. Ametani, Numerical analysis of power system transients and dynamics, 2015.

[7] W. Scott-Meyer, EMTP Rule Book Mode 31, B.P.A, Portland, Oregon, USA, 1982.

[8] H. Dommel, EMTP Theory Book, B.P.A, Portland, Oregon, USA, 1986.

[9] T. Noda, K. Takenaka, and T. Inoue, "Numerical integration by the 2-stage diagonally implicit Runge-Kutta method for electromagnetic transient simulations," IEEE Trans. Power Del., vol. 24, no. 1, pp. 390–399, 2008, doi: 10.1109/tpwrd.2008.923397.

[10] A. Ametani, Chapter 5 "XTAP", Numerical Analysis of Power System Transients and Dynamics, The Institution of Engineering and Technology (IET), 2015. [Online]. Available: https://www.xtap.org/

[11] A. Gole, Manitoba HVDC Research Centre. User's Guide on the Use of PSCAD, Winnipeg, Manitoba, Canada, 2004.

[12] H. Dommel, User's Manual for Program: Line Constants of Overhead Lines, B.P.A, Portland, USA, 1972.

[13] A. Ametani, "A general formulation of impedance and admittance of cables," IEEE Trans. Power Appar. Syst., vol. PAS-99, no. 3, pp. 902–910, 1980, doi: 10.1109/tpas.1980.319718.

[14] A. Ametani, T. Ohno, and N. Nagaoka, Cable system transients: Theory, Modeling and Simulation, John Wiley & Sons, 2015.

[15] A. Ametani, Cable Parameters Rule Book, B.P.A, Portland, Oregon, USA, 1994.

[16] S. A. Schelkunoff, "The Electromagnetic Theory of Coaxial Transmission Lines and Cylindrical Shields," Bell Syst. Tech. J., vol. 13, pp. 532–539, 1934.

[17] P. de Arizon and H. W. Dommel, "Computation of cable impedances based on subdivision of conductors," IEEE Trans. Power Del., vol. 2, no. 1, pp. 21–27, 1987, doi: 10.1109/tpwrd.1987.4308068.

[18] E. Comellini, A. Invernizzi, and G. Manzoni, "A computer program for determining electrical resistance and reactance of any transmission line," IEEE Trans. Power Appar. Syst., vol. PAS-92, no. 1, pp. 308–314, 1973, doi: 10.1109/tpas.1973.293628.

[19] R. Lucas and S. Talukdar, "Advances in finite element techniques for calculating cable resistances and inductances," IEEE Trans. Power Appar. Syst., vol. PAS-97, no. 3, pp. 875–883, 1978, doi: 10.1109/tpas.1978.354559.

[20] P. Graneau, Underground Power Transmission, John Wiley & Sons, New York, USA, 1979.

[21] R. Rivas and J. Marti, "Calculation of frequency-dependent parameters of power cables: matrix partitioning techniques," IEEE Trans. Power Del., vol. 17, no. 4, pp. 1085–1092, 2002, doi: 10.1109/tpwrd.2002.803827.

[22] M. Padilla, "El Método de Subdivisión de Conductores para Cables de Potencia Sectoriales," Master's thesis, CUCEI, Universidad de Guadalajara, Guadalajara, Jalisco, México, 2017.

[23] J. Ruiz, "Estimación de Transitorios en Cables de Potencia Mediante los Métodos de Subdivisión de Conductores y Elemento Finito," Master's thesis, CUCEI, Universidad de Guadalajara, Guadalajara, Jalisco, México, 2017.

[24] T. Miki and T. Noda, "An improvement of a conductor subdivision method for calculating the series impedance matrix of a transmission line considering the skin and proximity effects," IEEJ Trans. Power Energy, vol. 128, no. 1, pp. 254–261, 2008, doi: 10.1541/ieejpes.128.254.

[25] U. Schmidt, A. Shirvani, and R. Probst, "An improved algorithm for determination of cable parameters based on frequency-dependent conductor segmentation," in IEEE PES Transmission and Distribution Conf. Expo., 2012, pp. 1–7, doi: 10.1109/tdc.2012.6281601.

[26] F. A. Uribe and J. Flores, "Parameter estimation of arbitrary-shape electrical cables through an image processing technique," Electr. Eng., vol. 100, pp. 1749–1759, 2018, doi: 10.1007/s00202-017-0651-y.

[27] A. Cywiński and K. Chwastek, "Modeling of skin and proximity effects in multi-bundle cable lines," Progress in Applied Electrical Engineering (PAEE), pp. 1–5, 2019, doi: 10.1109/PAEE.2019.8788986.

[28] Y. Yin and H. Dommel, "Calculation of frequency-dependent impedances of underground power cables with finite element method," IEEE Trans. Magn., vol. 25, no. 4, pp. 3025–3027, 1989, doi: 10.1109/20.34358.

[29] COMSOL Multiphysics Reference Manual, version 5.3, COMSOL, Inc., [Online]. Available: www.comsol.com.

[30] A. Schött-Szymczak and K. Walczak, "Impact of cable configuration on the voltage induced in cable screen during work with one-sidedly ungrounded cable screen," Energies, vol. 14, p. 4263, 2021, doi: 10.3390/en14144263.

[31] H. Guan et al., "Simulation calculation for total electric field of three-phase power cable," in Proc. IEEE Int. Conf. High Voltage Eng. and Appl. (ICHVE), 2016, pp. 1–4, doi: 10.1109/ICHVE.2016.7800883.

[32] Y. Rangelov and D. Georgiev, "Short-circuit analysis in high-voltage transmission systems with a large share of underground cables," in Proc. 11th Electrical Eng. Faculty Conf. (BulEF), 2019, pp. 1–4, doi: 10.1109/BulEF48056.2019.9030751.

[33] L. Zhang, X. Tian, S. A. Boggs, and E. J. Bartolucci, "Determination of total resistive loss in a multiple circuit, three-phase cable system," IEEE Trans. Power Del., vol. 26, no. 3, pp. 1939–1945, 2011, doi: 10.1109/tpwrd.2011.2142199.

[34] Caio G. Morata, *et. al.*, "Frequency-dependent modeling of three-phase power cables for electromagnetic transient simulations", Int. Journal of Elec. Power & Energy Syst., Vol. 157, 2024, 109792, ISSN 0142-0615, https://doi.org/10.1016/j.ijepes.2024.109792.

[35] Tesfaye Nafo Tefera, *et. al.*, "Cable dimension determination using Finite Element Method Magnetic (FEMM) for three-core belted and gas

insulated cables", e-Prime - Advances in Electrical Engineering, Electronics and Energy, Vol. 10, 2024, 100826, ISSN 2772-6711, https://doi.org/10.1016/j.prime.2024.100826.
[36] MATLAB, version 9.3.0.713579 R2017b, Natick, MA: The MathWorks, Inc., 2017. [Online]. Available: www.matlab.com.
[37] F. A. Uribe, J. L. Naredo, P. Moreno, and L. Guardado, "Electromagnetic transients in underground transmission systems through the numerical Laplace transform," Int. J. Electr. Power Energy Syst., vol. 24, no. 3, pp. 215–221, 2002, doi: 10.1016/s0142-0615(01)00031-x.
[38] F. A. Uribe, O. Ramos-Leaños, and P. Zuniga, "An investigation of earth and sea-return impedances of power electrical cables," Electr. Power Syst. Res., vol. 223, p. 109608, 2023, doi: 10.1016/j.epsr.2023.109608.